Advanced Optical Materials

ADVANCED OPTICAL MATERIALS
www.advopticalmat.de

RESEARCH ARTICLE OPEN ACCESS

Spectral-Splitting Photovoltaic-Thermal Solar Collectors Using Selective Hybrid Liquid-Solid Optical Filters

Botho Lehmann[1] | Bryce S. Richards[1,2] | Gan Huang[1]

[1]Institute of Microstructure Technology, Karlsruhe Institute of Technology, Eggenstein-Leopoldshafen, Germany | [2]Light Technology Institute, Karlsruhe Institute of Technology, Karlsruhe, Germany

Correspondence: Gan Huang (gan.huang@kit.edu)

Received: 21 August 2025 | **Revised:** 5 February 2026 | **Accepted:** 5 February 2026

Keywords: hybrid optical filters | solar energy | spectral-splitting

ABSTRACT

Photovoltaic-thermal (PVT) solar collectors offer a promising solution for the co-generation of electricity and heat. Here, we investigate a spectral-splitting PVT collector that integrates a selectively-absorptive hybrid liquid-solid optical filter (LSOF). The LSOF offers a stable and efficient alternative to conventional nanofluid-based optical filters for spectral-splitting PVT collectors. Two photovoltaic (PV) configurations are examined—a silicon (Si) solar cell operated under non-concentrated sunlight, and a gallium arsenide (GaAs) solar cell operated under concentrated sunlight. A Fresnel lens with a geometric concentration ratio of 100 is employed to focus sunlight onto the LSOF, which selectively absorbs ultraviolet and sub-bandgap infrared radiation for heat generation. The remaining solar spectrum is transmitted to the PV cells for electricity generation. This configuration enables fluid temperatures of up to 86.8°C, while maintaining the PV cell temperature as low as 38.2°C, demonstrating effective thermal decoupling between the PV and solar thermal absorber. The PV cells have electrical efficiencies of 7.9% for the Si cell and 5.7% for the GaAs cell. Although the efficiency and output heat temperature of the current LSOF-based PVT collectors remain modest owing to optical losses and elevated temperatures, the system demonstrates the potential of hybrid optical filtering for solar co-generation.

1 | Introduction

The global demand for energy is driven by requirements for electricity and heat, accounting for approximately 20% and 50% of total energy consumption worldwide [1, 2]. Heat and electricity production remains reliant on fossil fuels in many regions. Mitigating emissions from these sectors is therefore critical to achieving international climate targets [3].

Solar energy is the most abundant and environmentally friendly energy resource and offers significant potential for the concurrent generation of heat and electricity via photovoltaicthermal (PVT) solar systems. The highest commercially available Si PV modules from SunPower currently achieve efficiencies of about 24% [4]. In real-world applications, standard test conditions are rarely met, as module operating temperatures often reach around 50°C, leading to a relative efficiency reduction of ∼6.8% due to the negative temperature coefficient of Si cells [4]. The remaining incident solar energy is mostly dissipated as heat. In a PVT solar collector, integration of a PV module with a thermal absorber enables capture of these thermal losses: the heat sink cools the PV cells, thereby lowering operating temperature and enhancing electrical output, while the recovered thermal energy is available for downstream applications. This effect results in combined system efficiencies that surpass those of standalone PV modules. For example, a SunPower PV module achieves an electrical efficiency of ∼24% at 25°C, whereas an Abora PVT collector delivers 18% electrical efficiency and 71% thermal efficiency at 25°C [5].

Commercially available PVT systems are primarily configured for low-temperature applications such as space heating. In these designs, the PV module is thermally coupled to a heat absorber to recover waste heat. However, the operating temperature of the PV cells and the delivery temperature of the thermal fluid are inherently linked, creating a trade-off between electrical performance and high-temperature heat output [6].

Advanced solar-concentrated spectral-splitting PVT technologies can potentially overcome this limitation by allowing for decoupling the PV and thermal absorber, although decoupling is not an inherent outcome of the approach, e.g., optical filters direct high-energy photons to the PV cells and lower-energy photons to the thermal absorber. This approach enables elevated thermal outputs at the expense of increased optical losses and increased system complexity [7]. Spectral-splitting PVT collectors offer advantages for the deep decarbonisation of heat and power generation [8]. Additionally, when employing concentrated PV cells, the increased irradiance elevates the open-circuit voltage, thereby enhancing electrical efficiency [8–10]. Recent advances in spectral-splitting PVT technologies are well summarised in several review articles [11, 7, 12–14]. Two main types of optical filters are employed in spectral-splitting PVT collectors: (1) Bragg-mirror-based filters [15–17], which are relatively mature and widely used in optics, and (2) selectively absorptive liquid-based filters [18, 19], which are still under development but offer dual functionality, i.e., spectral selectivity and direct heat transfer. The most common liquid-based optical filters are nanofluid optical filters. In these systems, metallic nanoparticles (e.g., silver, gold, aluminium) are engineered to absorb ultraviolet (UV) radiation, while the base fluid (e.g., water or heat transfer oils) absorbs infrared radiation. Taylor et al. pioneered the use of nanofluid filters in spectral-splitting PVT, demonstrating their potential as efficient, compact, and low-cost optical components [18]. Subsequent experimental studies by Liang et al. confirmed the spectral-splitting capabilities of Zinc oxide (ZnO) nanofluids [20, 21]. Many other nanoparticle-based nanofluids have been explored, including Ag/ZnO [22], polypyrrole [23], Carbon Nanotubes (CNT)/Ag [24], Au/ZnO [25], with additional examples reviewed in detail by Huang et al. [7] and Sajid et al. [26]. Ongoing research seeks to optimise nanofluids' spectral properties to approach the ideal filter, i.e., high absorption in UV (which cannot be used efficiently by PV cells) and infrared bands (which cannot be used by PV cells) for heating generation, and high transmittance in the visible and near-infrared for electricity generation [27]. However, current nanofluid filters face some limitations to be overcame, including inadequate spectral selectivity, optical losses from scattering, and long-term stability issues such as nanoparticle agglomeration [11, 7], which hinder overall system efficiency and highlight the need for improved filter designs.

In this study, we present a hybrid liquid-solid optical filter (LSOF) designed for spectral-splitting PVT collectors. The LSOF combines a UV–vis selective absorber film that targets wavelengths below 490 nm with a water layer whose absorption increases gradually from around 900–1400 nm. This configuration provides spectral selectivity, where useful visible and near-infrared light passes through for electricity generation, while unwanted ultraviolet and sub-bandgap infrared light is harvested as heat. We experimentally evaluate this system using two types of photovoltaic cells, Si and GaAs. Prototype solar collectors integrating the LSOF were fabricated and tested to assess their thermal and electrical performance under a dual lamp solar simulator.

2 | Results

2.1 | The Concept of Spectral-Splitting PVT Solar Collectors Employing Hybrid Liquid-Solid Optical Filters (LSOF)

We demonstrate the concept of a spectral-splitting PVT collector using a LSOF. This selectively absorptive approach employs a tailored optical filter to convert sub-bandgap infrared radiation, which cannot be used by photovoltaic (PV) cells, into heat, while also harvesting a portion of the high-energy UV–vis and short-wavelength visible light that PV cells convert inefficiently. The remaining portion of the solar spectrum is transmitted to the PV cells for electricity generation. This design, in combination with light concentration, reduces thermal stress on the PV cells and enables the collection of high-temperature heat without overheating the PV cell. As shown in Figure 1a, a Fresnel lens with a geometric concentration ratio of 100 concentrates sunlight onto the LSOF, which selectively absorbs a part of the solar spectrum for heat generation, and redirects specific spectral components to PV cells. The transmitted radiation is used by a non-solar-concentrated Si cell (effective area of 100 × 100 mm^2) as the Option 1, where the light is defocused by increasing the distance from the focal point. Alternatively, a gas-cooled solar-concentrated GaAs PV cell (effective area of 10 × 10 mm^2) is used as the Option 2, to generate electricity. In both Option 1 and Option 2 designs, the LSOF receives highly concentrated sunlight, enabling the generation of higher-temperature heat.

The structure of the LSOF is detailed in Figure 1b. It comprises a 10-mm-thick water layer enclosed by a 1-mm-thick fused silica top cover and a 1-mm-thick UV–vis selective absorber layer at the bottom. The housing is made of polymethylmethacrylate, with silicone gaskets sealing the water layer. The LSOF chamber has two ports on the side walls. One port serves as a thermocouple port, allowing thermocouple cables to pass into the middle of the LSOF to measure its internal temperature; the other serves as an expansion valve to reduce the risk of breakage during the heating process due to water expansion.

As shown in Figure 1c, the water layer absorbs infrared radiation beyond a cutoff wavelength λ_H (~1100 nm), taking advantage of water's strong absorption in this spectral range, along with its high heat capacity and non-toxic, low-cost properties. The UV–vis selective absorber is a commercially available optical filter that absorbs light with wavelengths below λ_L, around 490 nm in this study. As a result, the LSOF is highly transparent to the spectral band between λ_L and λ_H, while absorbing the remainder for thermal use. The LSOF therefore functions simultaneously as an optical filter and as a thermal absorber.

According to a previous theoretical analysis, the optimal selection of λ_L depends on the weighting coefficient w, which reflects the relative value of thermal energy compared to electricity [28]. This coefficient can be defined in thermodynamic terms

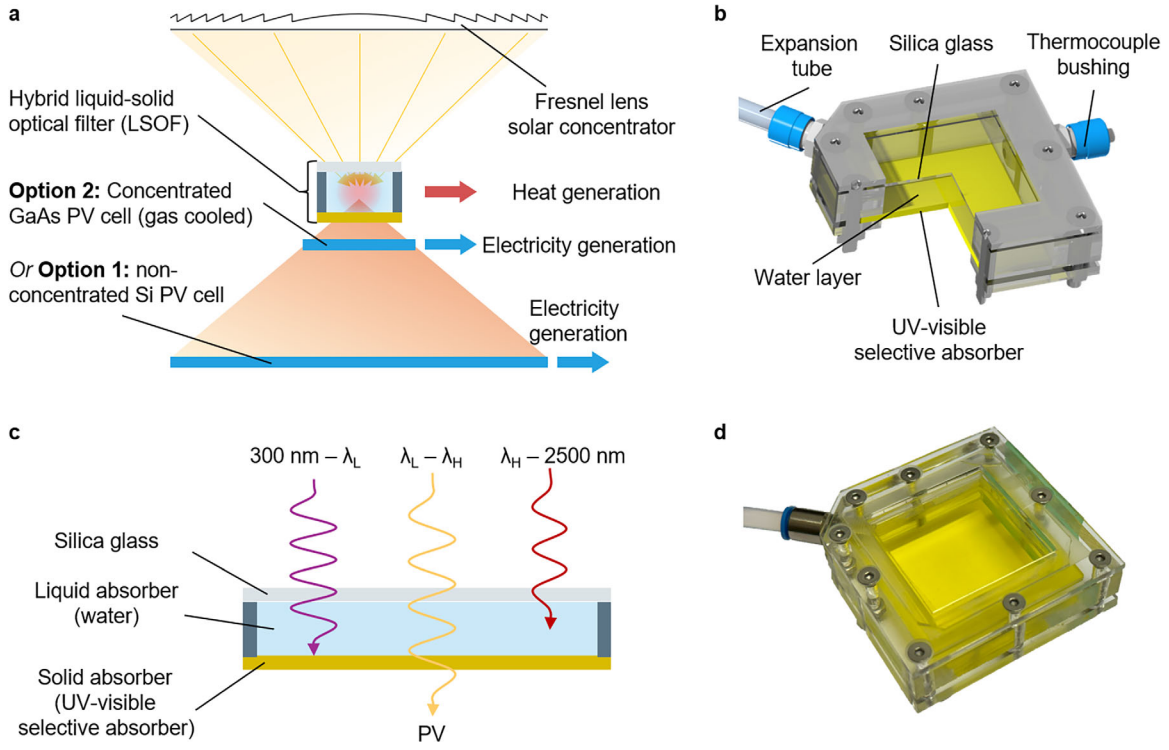

FIGURE 1 | Design concept and experimental implementation of the spectral-splitting PVT solar collector using a hybrid liquid-solid optical filter (LSOF). a) Schematic of the spectral-splitting PVT system, in which a Fresnel lens concentrates sunlight onto the LSOF. The LSOF selectively absorbs parts of the solar spectrum for thermal energy harvesting at high temperature, while transmitting the remaining wavelengths to either a non-concentrated silicon (Si) PV cell by defocusing or a gas-cooled concentrated gallium arsenide (GaAs) PV cell for electricity generation. b) Structure of the LSOF, consisting of a 1-mm-thick fused silica plate, a 10-mm-thick water layer, and a 1-mm-thick UV–vis selective absorber, enclosed within a polymethylmethacrylate frame. c) Spectral absorption scheme of the LSOF. The UV–vis selective absorber filters out wavelengths below λ_L to reduce parasitic ultraviolet heating, while the water layer absorbs infrared radiation above λ_H, contributing to high-temperature thermal output. The spectral window between λ_L and λ_H is transmitted to the PV cell for efficient electricity generation. d) Photograph of the fabricated LSOF integrated into the experimental setup.

(e.g., using second-law efficiency or Carnot factors), economic terms (e.g., cost ratio of heat to electricity), or environmental metrics (e.g., emissions reductions). For example, as w decreases, thermal energy becomes less valuable, and the optimal λ_L shifts toward shorter wavelengths to allocate less of the spectrum to heat generation.

In this proof-of-concept study, we intentionally select $\lambda_L = 490$ nm to represent an application scenario in which thermal energy has a relative value of 30%–40% compared to electricity ($w = 0.3$–0.4) [28]. This weighting corresponds directly to several realistic use cases. For example, it is consistent with heat supplied by an air-source heat pump with a coefficient of performance of $COP = 1/w$, i.e., 2.5–3.3, which lies within the typical operating range of widely deployed air-source heat pumps for space and water heating [29]. It also aligns with industrial low- to mid-temperature heat demand at 425–500 K when evaluated based on thermodynamic value via the Carnot factor. Furthermore, this weighting is representative of real energy-price conditions; for instance, in Denmark in 2024, the price of natural gas for heating was approximately 1.13 DKK/kWh compared to 2.8 DKK/kWh for electricity [30], corresponding to a w value of around 0.4.

It should be emphasised that $\lambda_L = 490$ nm is used here solely to demonstrate the proof-of-concept of our spectral-splitting hybrid solar collector in this study. This value is not necessarily optimal, but reflects the specific application scenario described above. Both λ_L and w can be adjusted to suit different application contexts.

Figure 1d shows a photograph of the fabricated LSOF. For comparison, we also built and tested a reference water optical filter (WOF), consisting of a 10-mm-thick water layer enclosed between two 1-mm-thick fused silica plates, without the UV–vis selective absorber. Details of the WOF design are provided in Figure S1. To minimise conductive and radiative heat losses, both the LSOF and WOF chambers were thermally insulated using extruded polystyrene foam wrapped in aluminium foil.

In the concentrated-PV configuration, the GaAs cell was encapsulated between a 0.5-mm-thick fused silica cover and a 0.5-mm-thick copper mounting plate, bonded with polydimethylsiloxane. An infrared temperature sensor was used to monitor the back surface temperature of the encapsulated GaAs cell, as shown in Figure S2. To provide active cooling, nitrogen gas was flushed across the rear surface at a flow rate of 25 L/min. For the Si cell, temperature was monitored using a thermocouple mounted at the back, as shown in Figure S3. All components were arranged to operate within the spatial constraints of a dual-lamp (xenon/halogen) solar simulator.

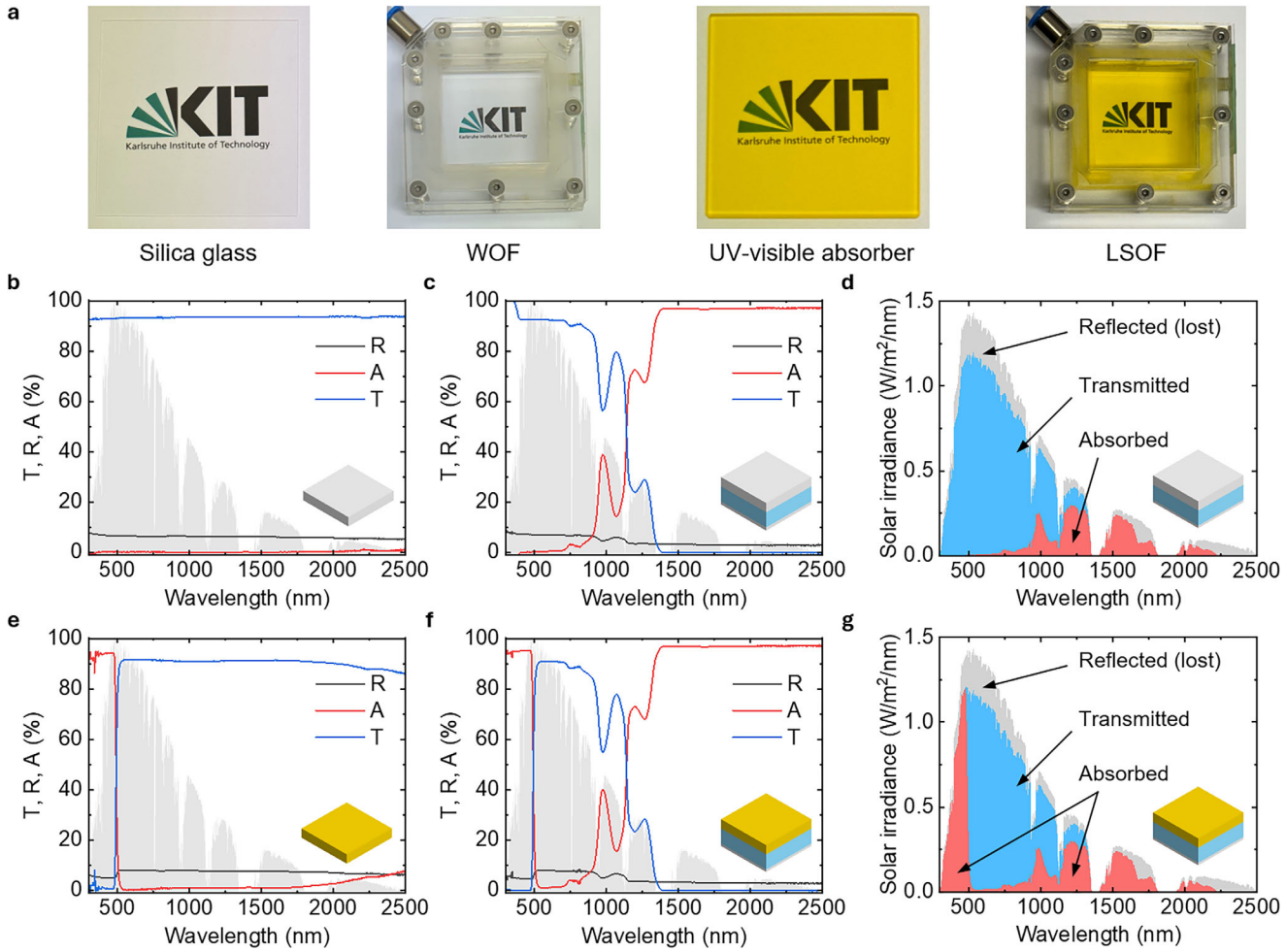

FIGURE 2 | Optical properties of optical components in the spectral-splitting PVT solar collectors. a) Photographs of the optical components (fused silica, WOF, UV–vis absorber, and LSOF) placed in front of the KIT logo for visual comparison. b) Measured transmittance of the fused silica, showing high and uniform transmission (93.0%) across the full solar spectrum (300–2500 nm) with negligible absorption or reflection. c) Optical characterisation of the WOF. It exhibits high transmittance below 900 nm and strong absorption above 1400 nm. d) Spectral-splitting performance of the WOF under AM 1.5D, indicating the fraction of irradiance absorbed for heat, transmitted to the PV cell, and lost to optical reflections. e) Measured optical properties of the UV–vis selective absorber, demonstrating a sharp cutoff near 490 nm and optical properties similar to WOF in the longer wavelength range. f) Measured optical properties of LSOF. The LSOF well combines the selective optical filtering of the water layer and the UV–vis selective absorber. g) Beam splitting effect of the LSOF under AM 1.5D, showing enhanced thermal absorption and clear spectral division between heat and electricity channels, along with quantified optical losses.

2.2 | Optical Characterisation of Optical Components in the Spectral-Splitting PVT Solar Collectors

The optical performance of each component utilised in our spectral-splitting PVT collector is characterised using a UV–vis-NIR spectrophotometer, with transmittance, absorptance, and reflectance measurements detailed in the Methods section. These measurements enable quantitative evaluation of beam splitting efficiency. Figure 2a displays photographs of the optical components, from left to right, i.e., fused silica, WOF, UV–vis selective absorber, and LSOF. The fused silica and WOF are visibly transparent, whereas the UV–vis selective absorber and the LSOF appear semi-transparent yellow. As shown in Figure 2b, fused silica exhibits high and uniform transmittance across the solar spectral range (300–2500 nm), with a spectrally weighted transmittance of 93.0% and negligible selective absorption throughout the measured wavelength range. Figure 2c illustrates the selective spectral transmittance and absorption characteristics of the WOF. The transmittance remains high (90.7%) within the 300–900 nm range and then declines as the wavelength increases, approaching opacity beyond 1400 nm. This behaviour is attributable to the strong vibrational absorption bands of water molecules, enabling selective absorption of most infrared radiation starting from 900 nm. The spectral-splitting effect of the WOF under the AM 1.5D solar spectrum (representing direct normal sunlight at an air mass of 1.5), where only the direct component is considered because it is the portion of the solar spectrum that can be concentrated, considering the transmission through the Fresnel lens, is detailed in Figure 2d. The solar spectrum is effectively divided into two distinct components. The WOF transmits 87.6% of radiation within 300–1100 nm suitable for Si solar cells, and 90.9% within 300–870 nm ideal for GaAs solar cells. In total, the WOF absorbs 15.7% of the incident radiation for thermal

harvesting, while optical losses from reflections (Fresnel lens and WOF surfaces) account for 18.0%. With an effective optical area of 38 × 38 mm^2 and a total incident solar radiation power of 8.9 W, this results in 1.4 W absorbed for thermal use, 5.9 W transmitted to the PV cells, and 1.6 W lost optically.

Figure 2e reveals the optical characteristics of the UV–vis selective absorber, which strongly absorbs (92.5%) wavelengths below ~490 nm. Photons in this high-energy region exceed the bandgap energy of typical Si and GaAs PV cells, leading to significant thermalisation losses and reduced electrical conversion efficiency. Thus, converting this UV–vis spectrum portion directly into heat through absorption is more beneficial than photovoltaic conversion. As depicted in Figure 2f, the LSOF integrates the spectral selectivity of both the water layer and the UV–vis selective absorber, achieving a well-defined and efficient beam splitting performance. The relative uncertainty of the transmittance is less than 1 rel.%. Figure 2g quantifies this effect, demonstrating sharp spectral separation. The Si solar cell exhibits an effective spectral response from approximately 300–1100 nm, whereas the GaAs solar cell responds over a narrower range of approximately 300–870 nm. Based on the optical properties of LSOF, 83.8% of the radiation within the 490–1100 nm range is transmitted for Si solar cells, and 87.6% within 490–870nm is transmitted for GaAs solar cells. The LSOF absorbs 29.2% of the incident radiation for thermal energy, while optical reflection losses remain constant at approximately 18.0%. Given the same effective area as WOF and incident irradiance (8.9 W), the LSOF absorbs 2.6 W for heat, transmits 4.7 W to the PV cells, and loses 1.6 W optically.

Considering these optical properties, the presence of the WOF slightly reduces the electrical efficiency of the Si solar cell due to infrared absorption in 900–1100 nm range. Conversely, the GaAs cell remains largely unaffected since its bandgap (~870 nm) lies outside the primary absorption range of water. The introduction of the UV–vis selective absorber further decreases the electrical efficiency for both Si and GaAs cells but significantly enhances thermal energy capture. In general, water serves as an effective, low-cost, and environmentally friendly infrared absorber, although it lacks a sharp cutoff wavelength. In contrast, the UV–vis selective absorber provides a precise spectral cutoff in the UV–vis region, complementing the infrared absorption of water and enabling comprehensive beam splitting.

The Fresnel lens, made of polymethylmethacrylate, matches the transmittance of polymethylmethacrylate plate across the solar spectrum, with a spectrally-weighted transmittance of 88.5%. Experimental tests reveal that placing the Si PV cell directly behind the Fresnel lens reduces its electrical efficiency to approximately 92% compared to the efficiency measured without the Fresnel lens, aligning well with the measured transmittance characteristics of polymethylmethacrylate in the active range of the Si PV cell. However, angular optical losses increase at the lens edges due to steep micro-groove angles.

2.3 | Performance of the Spectral-Splitting PVT Collector Based on a Non-Concentrated Si PV Cell

To investigate the electrical and thermal performance of the spectral-splitting PVT collector using a Si PV cell (Option 1 in Figure 1a), we design and fabricate a prototype, as shown in Figure 3a. A Fresnel lens with an area of 100 × 100 mm^2 and a focal length of 90 mm is positioned above the system to concentrate sunlight from a solar simulator. The WOF or LSOF optical filter is placed at the lens's focal point. The Si PV cell, with an effective area of 100 × 100 mm^2, is positioned 160 mm below the Fresnel lens, where it achieves maximum power output and is arranged with some surrounding space to allow natural convection cooling, as shown in Figure S4. The overall dimensions of the test rig for the spectral-splitting PVT collector based on a non-concentrated Si PV cell (Figure 3a) are 100 × 100 × 160 mm (width × depth × height). The Fresnel lens is required to generate high irradiance at the LSOF for thermal harvesting. The Si PV cell itself operates under de-focused, non-concentrated illumination, ensuring near one-sun conditions while enabling high-temperature heat generation upstream.

Thermal efficiency is determined by recording the transient temperature change in the water chamber at a frequency of 1 Hz, as shown in Figure 3b for the WOF and Figure 3c for the LSOF. The transient temperature refers to the time-dependent temperature evolution of the optical filters during heating under illumination, which is used to determine the thermal performance of the system. The slope of the temperature-time curve is used to calculate thermal efficiency based on the water chamber's heat capacity, as described in the Methods section. The LSOF configuration reaches a higher peak temperature (86.8°C) compared to the WOF (82.1°C), owing to greater absorption of UV–vis radiation. Compared with conventional nanofluid-based optical filters in spectral-splitting PVT collectors, the LSOF achieves comparable or higher heat-generation temperatures without relying on nanoparticle suspensions. Reported heating temperatures in the literature include ~50°C for ZnO nanofluids [20, 21], ~80°C for Ag–ZnO hybrid nanofluids [22], ~70°C for polypyrrole nanofluids [23], and ~60°C for CNT–Ag hybrid nanofluids [24].

Consistent with this mechanism, the maximum Si PV cell temperature in the LSOF setup is 38.4°C, slightly lower than 41.5°C observed with the WOF, owing to less waste heat in the Si PV cell in the LSOF setup. Minor fluctuations in PV cell temperature are due to current-voltage (I-V) measurements conducted every 10 min, during which power extraction altered the thermal equilibrium of the cell.

Temperature fluctuations are observed in the WOF configuration, as shown in Figure 3a, and are attributed to the formation of small gas bubbles around the thermocouple, as illustrated in Figure S5. These bubbles begin to form at temperatures of approximately 70°C and locally insulate the thermocouple, impairing heat transfer and leading to fluctuations in the measured temperature. In contrast, the temperature evolution in the LSOF configuration is smooth, as shown in Figure 3b. Although small gas bubbles also form in the LSOF, they do not accumulate around the thermocouple (Figure S5). As a result, the presence of small gas bubbles has only very slight impact on the overall thermal performance of the optical filters, and temperature fluctuations occur only when bubbles directly surround the thermocouple, leading to localized measurement artefacts.

Figure 3d presents IV curves for various configurations. The Si PV cell without the Fresnel lens and filters achieves the

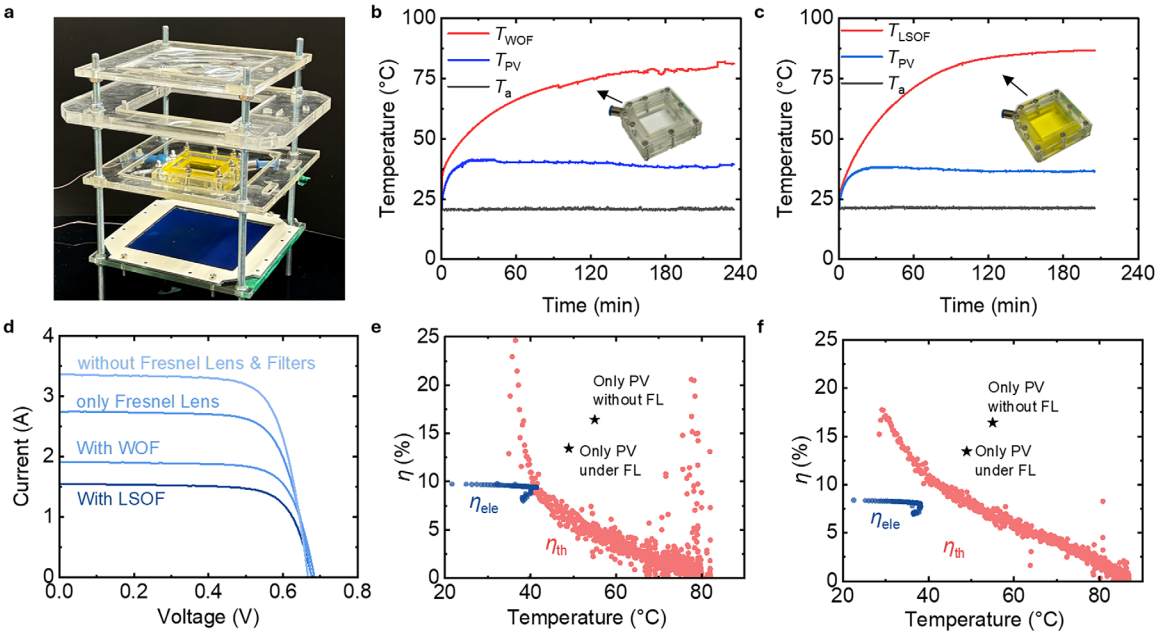

FIGURE 3 | Electrical and thermal performance of the spectral-splitting PVT collector using a Si PV cell with WOF and LSOF configurations. a) Experimental setup showing the Si PV cell with the Fresnel lens and the LSOF optical filter. b) Heating curves of the WOF-based spectral-splitting PVT collector. c) Heating curves of the LSOF-based spectral-splitting PVT collector. Water reaches a higher temperature due to increased absorption in the UV–vis range, while the PV cell temperature remains lower due to reduced irradiance in non-contributing spectral bands. d) Current-voltage (I-V) curves of the Si PV cell under different configurations. The bare cell exhibits the highest output, while the addition of the Fresnel lens, WOF, and especially LSOF introduces progressive losses. e) Electrical and thermal efficiencies of the WOF-based spectral-splitting PVT collector, compared to the bare PV cell, with electrical efficiency plotted as a function of PV cell temperature and thermal efficiency plotted as a function of WOF temperature. f) Electrical and thermal efficiencies of the LSOF-based spectral-splitting PVT collector, over their respective temperatures. The LSOF demonstrates improved thermal performance but reduced electrical efficiency relative to the WOF, consistent with its optical absorption characteristics.

highest electrical efficiency of 16.4%. The addition of optical elements, such as the Fresnel lens, WOF, or LSOF, resulted in reduced electrical output due to optical losses. While the open-circuit voltage is only slightly affected, the short-circuit current experienced significant reduction, due to the lower light intensity on the PV cell in its active range. Losses observed between the bare cell and the Fresnel-only configuration are due to Fresnel lens absorption, reflection, and misalignment. Further losses with the WOF stemmed from fused silica reflection and water absorption in the 900–1100 nm range. Transitioning to the LSOF introduces additional losses via UV–vis absorber absorption.

The electrical and thermal efficiencies of the WOF-based spectral-splitting PVT collector as a function of temperature are shown in Figure 3e. The electrical efficiency is 9.7% at 21.7°C, decreasing to a stable efficiency of 9.4% at 41.5°C. Thermal efficiency is 10.1% at 40°C but declined to 4.0% at 60°C due to increased heat loss to the ambient environment. In comparison, the LSOF-based collector demonstrated higher thermal but lower electrical efficiency, as shown in Figure 3f. The electrical efficiency is 8.4% at 22.6°C, decreasing to a stable value of 7.9% at 38.2°C, while thermal efficiency reaches 11.1% at 40.0°C and 5.8% at 60°C. These results are consistent with the optical properties of the WOF and LSOF. At elevated temperatures in both the WOF and LSOF configurations, the formation of small gas bubbles leads to increased scattering and diffusion of incident sunlight away from the active PV area. As a result, the irradiance reaching the PV cell is reduced, leading to decreases in both PV cell temperature (as shown in Figure 3b,c) and electrical efficiency (as shown in Figure 3e,f). The bubble-induced light diffusion causes an approximately 14 rel.% reduction in PV electrical efficiency in both configurations.

The bare Si PV cell exhibits an electrical efficiency of 16.4% at an operating temperature of 55.0°C, which is significantly lower than the datasheet efficiency at the standard test condition (STC) of between 21.8 to 22.5% due to some mismatch in the solar simulator's spectrum; elevated cell temperature from 25°C to 55°C; and imperfect manual soldering of cables to the solar cells. The Si PV cell temperatures in the WOF and LSOF configurations were significantly lower (41.5°C and 38.2°C, respectively), owing to reduced thermal load. However, the corresponding electrical efficiencies drop to 9.4% and 7.9%, representing relative reductions of 42.7% and 51.8%, respectively. These declines are consistent with the optical losses observed in each configuration.

Specifically, in the WOF configuration, the Fresnel lens accounts for 42.6 rel.% of the total losses for the PV cell, while the hybrid spectral-splitting absorber contributes to 57.4 rel.%. In the LSOF configuration, the corresponding contributions are 35.1 and 64.9 rel.%, respectively. Although both the WOF and LSOF configurations gain thermal output, the thermal gain is roughly comparable to the electrical loss resulting from added optical elements. Thus, minimising optical losses remain critical. Strategies such as applying anti-reflective coatings or designing alternative liquid compositions better matched to Si PV absorption characteristics should be considered to enhance overall system efficiency.

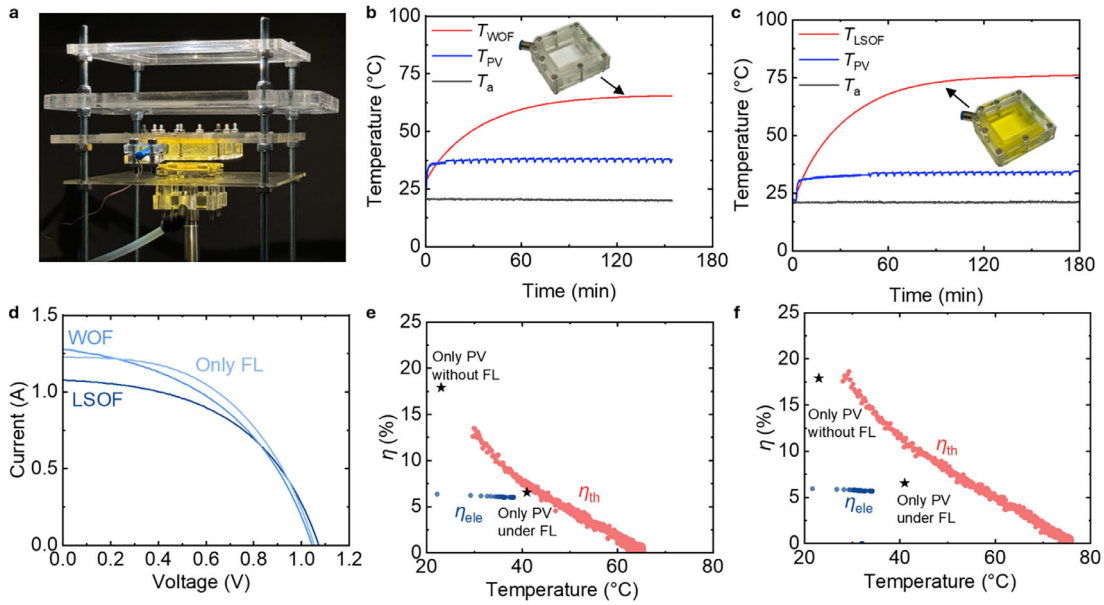

FIGURE 4 | Electrical and thermal performance of the spectral-splitting PVT collector using a GaAs PV cell with WOF and LSOF configurations. a) Experimental setup showing the GaAs PV cell positioned at the focal point of the Fresnel lens. b) Heating curves of the WOF-based spectral-splitting PVT collector. c) Heating curves of the LSOF-based spectral-splitting PVT collector. Water reaches higher temperatures due to additional absorption in the UV–vis range, while the PV cell remains cooler. d) I-V curves of the GaAs PV cell. The WOF configuration shows minimal electrical loss, while the LSOF introduces more significant current loss due to absorption in the 300–490 nm range. e) Electrical and thermal efficiencies of the WOF-based spectral-splitting PVT collector, with electrical efficiency plotted as a function of PV cell encapsulation temperature and thermal efficiency plotted as a function of WOF temperature. f) Electrical and thermal efficiencies of the LSOF-based spectral-splitting PVT collector, over their respective temperatures. The LSOF achieves higher thermal efficiency but reduced electrical output, consistent with its stronger spectral absorption.

2.4 | Performance of the Spectral-Splitting PVT Collector Based on a Concentrated GaAs PV Cell

The water layer in the WOF and LSOF optical filters absorbs part of the solar spectrum in the 900–1100 nm range, which reduces the electrical efficiency of the Si PV cell due to its bandgap wavelength of approximately 1100 nm. To minimise this spectral mismatch, we also select and test a GaAs PV cell in the spectral-splitting PVT collector, as the bandgap wavelength of GaAs is around 870 nm, below which the water layer remains highly transparent.

To investigate the electrical and thermal performance of the spectral-splitting PVT collector using a GaAs PV cell (Option 2 in Figure 1a), we design and fabricate a prototype, shown in Figure 4a. The GaAs PV cell is positioned at the focal point (90 mm) of the Fresnel lens (100 × 100 mm^2) and has an active area of 10 × 10 mm^2, resulting in a geometric concentration of 100. In this configuration, the absorber chamber is placed slightly in front of the focal point, resulting in a reduced concentration ratio on the optical filters compared to the Si-based configuration. Additional thermal insulation layers (not shown in Figure 4a) are wrapped around the optical filter, as shown in Figure S6. Flowing nitrogen gas at a flow rate of 25 L/min flushes the back of the GaAs PV cell for cooling, as shown in Figure S2. The overall dimensions of the test rig for the spectral-splitting PVT collector based on a concentrated GaAs PV cell (Figure 4a) are 100 × 100 × 90 mm (width × depth × height).

To determine thermal efficiency, we measure the transient temperature change, shown in Figure 4b for the WOF and Figure 4c for the LSOF. The LSOF reaches a higher peak temperature (76.0°C) compared to the WOF (65.5°C), due to greater absorption in the UV–vis spectrum. The measured maximum temperature on the back of the encapsulated GaAs PV cell in the LSOF configuration is 34.6°C, lower than the 38.5°C observed in the WOF configuration. Minor fluctuations in PV cell temperature occur during IV curve measurements taken at 10-min intervals, as power extraction momentarily alters the cell's thermal equilibrium.

It is important to note that under concentrated sunlight, the actual temperature of the GaAs cell is significantly higher than the temperature measured at the back of the encapsulated module due to thermal resistance. As shown in Figure S7, the GaAs cell can be 30°C–50°C hotter than the measured backside temperature under the solar concentration. Bubble formation is minimal in this configuration, primarily due to lower optical filter temperatures. No bubbles form in the WOF setup, consistent with prior observations at or below 65°C. In the LSOF configuration, minor bubble formation appears above 70°C but does not occur near the thermocouple, minimising its thermal impact. Additionally, the reduced light concentration (30 × 30 mm^2 compared to 17 × 17 mm^2) mitigates hotspot formation at the thermocouple, contributing to overall stability, as shown in Figure S5.

Figure 4d shows IV curves for various configurations. As with the Si-based system, adding optical filters (WOF or LSOF) introduces unavoidable optical losses. However, the WOF filter has minimal impact on electrical performance since both the fused silica and water layer are highly transparent in the spectral range below 870

nm. Transitioning from WOF to LSOF leads to further losses due to UV–vis absorber absorption.

Electrical and thermal efficiencies of the WOF-based configuration as a function of water temperature are shown in Figure 4e. Electrical efficiency is 6.3% at 22.2°C, decreasing to a stable value of 6.0% at 38.2°C. Thermal efficiency reaches 7.5% at 40°C and drops to 1.5% at 60°C due to increasing thermal losses to the ambient. Compared to WOF, the LSOF configuration, shown in Figure 4f, achieves higher thermal efficiency but lower electrical efficiency. Electrical efficiency is 5.9% at 21.7°C, decreasing slightly to a stable value of 5.7% at 34.2°C, with thermal efficiencies of 11.7% at 40°C and 4.9% at 60°C.

The bare, non-concentrated GaAs PV cell used in this study achieves an electrical efficiency of 17.9% under the solar simulator at an operating temperature of 22.0°C. Under concentrated illumination, however, the electrical efficiency decreases significantly to 6.5%, corresponding to a relative reduction of 63.7%. This reduction can be attributed to three primary factors: (i) a 9.9 rel.% loss due to optical attenuation by the Fresnel lens and fused silica cover, based on measured optical properties; (ii) a 30.2 rel.% loss resulting from elevated cell operating temperatures under concentrated sunlight, estimated using the temperature coefficient of GaAs PV cells [31–33]; and (iii) a 23.6 rel.% loss caused by optical misalignment between the Fresnel lens and the small-area GaAs cell. These results indicate that improved thermal management and more precise optical alignment are critical for enhancing electrical performance in future designs.

In the literature, GaAs electrical efficiencies of approximately 8% have been reported for spectral-splitting PVT collectors operating at around 60× concentration ratios [34]. However, it should be noted that state-of-the-art non-concentrated single-junction GaAs solar cells can achieve efficiencies of approximately 25%, while concentrated multi-junction GaAs devices can reach efficiencies of around 35% [35]. Therefore, the use of higher-quality GaAs PV cells, specifically designed for concentrated operation, represents a clear pathway for further improving electrical performance in spectral-splitting PVT systems.

At their respective peak temperatures, the GaAs PV cells in the WOF- and LSOF-based configurations exhibit electrical efficiencies of 6.0% and 5.7%, respectively; 7.7% and 12.3% lower than the solar-concentrated GaAs PV cell without optical filters. The WOF filter has minimal impact on efficiency due to its high transmittance (~90.9%) in the 300–870 nm range. By contrast, the LSOF filter significantly reduces electrical efficiency by absorbing the 300–490 nm portion of the spectrum. Overall, compared to the Si-based configuration, both WOF and LSOF exert less influence on the electrical performance in the GaAs-based system, while still enabling meaningful thermal energy recovery. In future work, improving PV cell alignment is critical for further enhancing electrical efficiency.

The LSOF was exposed to 100× high-concentrated light for a cumulative duration of around 20 h during the experiments. After the high-concentration light testing, the optical properties of the LSOF were measured again and compared with its original optical properties. The results show that the optical properties remain nearly unchanged after the 20 h exposure (Figure S8), demonstrating the good optical stability of the LSOF.

3 | Conclusion

This study demonstrates the feasibility and performance potential of spectral-splitting photovoltaic-thermal (PVT) collectors incorporating hybrid liquid-solid optical filters (LSOF) for thermal–electrical decoupling. By integrating a UV–vis selective absorber with a water-based optical chamber, the LSOF enables effective spectral filtering: high-energy and sub-bandgap photons are redirected for thermal use, while the remaining spectrum is transmitted to photovoltaic (PV) cells for electricity generation. This strategy successfully lowers PV cell temperature while enhancing thermal energy harvesting.

For the Si PV cell under solar concentration, electrical efficiency decreases from 13.4% (no optical filter) to 9.4% with the water optical filter (WOF), and further to 7.9% with the LSOF. These losses correlate directly with the spectral absorption characteristics of the filters, i.e., infrared absorption above 900 nm by the WOF and additional UV–vis absorption below 490 nm by the LSOF. Despite these reductions, thermal efficiency increases significantly, with steady-state fluid temperatures reaching 86.8°C in the LSOF configuration and 82.1°C with the WOF. For the GaAs PV cell, which has a shorter bandgap wavelength (~870 nm), the WOF imposes only a slight reduction in electrical efficiency (6.5%–6.0%), due to its high transparency in the relevant spectral range. The LSOF reduces electrical efficiency further to 5.7% by absorbing short-wavelength radiation but simultaneously increases thermal output. Although the absolute electrical performance of the GaAs cell remains lower than expected, primarily due to alignment sensitivity and elevated cell temperatures under concentration, the GaAs-based configuration confirms the value of spectral selectivity in tailoring system performance to specific PV materials.

Overall, this work validates the spectral-splitting approach for thermally decoupling the PV and thermal components of PVT systems. The LSOF presents an alternative to nanofluid-based filters, with advantages in stability, tunability, and optical clarity. While the current system exhibits reduced electrical performance compared to standalone PV modules, it opens a promising path toward hybrid solar energy utilisation.

The thermal efficiency of both spectral-splitting PVT collectors is low at elevated operating temperatures, particularly above 60°C, due to increased convective and radiative heat losses to the ambient environment. In the present laboratory-scale prototype, these losses are further amplified by limited thermal insulation of the WOF and LSOF chambers. Future designs should therefore incorporate improved thermal insulation (e.g., vacuum insulation), optimized flow or heat-extraction strategies, and anti-reflective or low-emissivity surface treatments to mitigate optical and thermal losses at high operating temperatures. Regarding scalability, the LSOF concept relies on commercially available materials and simple planar geometries, indicating good potential for scale-up to larger-area collectors. However, translating the current lab-scale demonstration to practical installations will require system-level optimization, including improved optical alignment,

modular filter integration, and validation under realistic outdoor operating conditions.

The LSOF represents an alternative to nanofluid-based spectral filters for spectral-splitting PVT applications. The hybrid liquid–solid design enables stable spectral filtering using commercially available materials and simple planar geometries, while avoiding the need for nanoparticle dispersion control (nanoparticle agglomeration or long-term optical degradation). Nanofluid-based filters, on the other hand, offer high tunability and have demonstrated promising performance in various configurations. Although a detailed levelized cost analysis is beyond the scope of this proof-of-concept study, the present results suggest that LSOF-based systems warrant further investigation from a system-level and techno-economic perspective in future work.

4 | Method

4.1 | Prototype Fabrication

The Fresnel lens is made of polymethylmethacrylate, with a surface area of 100 × 100 mm^2 and a focal length of 90 mm (*Six Seasons*). The fused silica components are cut from a 5-inch fused silica wafer (*Wafer Universe*). The UV–vis selective absorber is a commercially available optical filter (*JB490 type, Shenzhen Infrared Laser Technology*). The silicon (Si) solar cell is a C60 model from *SunPower* [36]. Electrical contacts are manually soldered, which introduces a degree of contact resistance and minor performance loss. The gallium arsenide (GaAs) solar cell is obtained from *XiaYi Solar*. The frames of both the water optical filter (WOF) and the liquid-solid optical filter (LSOF) are fabricated from polymethylmethacrylate. The entire prototype structure, including optical filter chambers and supporting frame, is made of PMMA and is designed to be mountable on the platform of the solar simulator (*class AAA, Wacom)*.

4.2 | Optical Characterisation

To comprehensively characterise the optical properties of each component, a UV-Vis-NIR spectrophotometer (*Agilent Cary 7000*) was used. Spectral measurements were taken across the 250 nm to 2500 nm range in 10 nm intervals. The spectral absorption was determined from the measured reflectance and transmittance. To assess the total absorbed power in the liquid absorber and in the PV cell, as well as the weighted transmittance and absorption, the recorded spectral data were multiplied pointwise with the AM1.5D solar spectrum (900 W/m^2). This procedure allowed for accurate quantification of spectrally resolved absorption under standard direct irradiance conditions.

4.3 | Electrical Characterisation

The electrical performance of both the Si and GaAs PV cells was evaluated using a continuous dual-lamp (xenon/halogen) solar simulator (*class AAA, Wacom*) in combination with a high-precision source meter (*Keithley 2618B*). To replicate the solar spectrum and irradiance conditions, a dual-light source consisting of a xenon arc lamp (*Wacom KXL-500F*) and a halogen lamp (*Ushio JC-36V-400W*) was employed. The solar simulator is calibrated to approximate the AM1.5G solar spectrum; however, some spectral mismatch remains. The detailed spectral distribution of the simulator output is shown in Figure S9. All the experiments in this study were conducted under the solar simulator with AM1.5G spectrum (1000 W/m^2). Due to the ±3.0 A current limitation of the source meter within the operating voltage range, shading was required during standalone measurements of the Si PV cell to avoid saturation caused by its high short-circuit current. I-V curves were obtained by sweeping the voltage from 0 V to the open-circuit voltage (V_{OC}) in increments defined by the specific characteristics of the cell under test. The electrical efficiency is calculated based on the electrical power output of the PV cell relative to the total direct irradiance of the solar simulator. For the Si PV cell, the voltage step size was initially set to 0.04 V, with measurements recorded every 25 s for the first 40 min. After thermal stabilisation of the PV cell, the step size was reduced to 0.01 V, and the measurement interval was increased to 10 min to capture long-term behaviour under steady-state conditions. The GaAs PV cell, operating under higher light concentration and exhibiting rapid thermal response, required shorter measurement intervals and a more targeted voltage range. Initially, measurements were performed every 16 s by sweeping the voltage from 0.4 V to V_{OC} in steps of 0.05 V. In the experiment with the selective absorber, the protocol included 35 repetitions at 16-s intervals, followed by 30 measurements at 60-s intervals with a voltage sweep from 0 V to V_{OC} and a step size of 0.05 V. Finally, the system was monitored at 5-min intervals with a finer step size of 0.01 V over the full voltage range. Based on the results of this initial experiment, the protocol was adapted for the IV configuration. Here, IV curves were recorded 45 times at 16-s intervals using a 0.05 V step size over the 0.4 V to V_{OC} range. Subsequent measurements were performed every 5 min with a 0.01 V step size across the full voltage range, which proved sufficient to capture the dynamic and steady-state electrical behaviour of the system.

4.4 | Thermal Characterisation

The thermal performance of the system was evaluated by continuously monitoring the temperatures of the water chamber and the photovoltaic cells. For the Si PV cell and water chamber, Type T thermocouples (measurement range: −200°C to 260°C) were connected to a Pico Technology TC-08 data logger to record temperature data with a sampling rate of 1 Hz. For the GaAs PV cell, temperature measurements were taken using an IR temperature sensor (*Optris GEN CSS LE*), positioned to monitor the back surface of the encapsulated cell. To improve measurement accuracy, the rear surface was coated with black spray paint to enhance emissivity and therefore reduce noise. Calibration of the IR sensor was performed by simultaneously heating the encapsulated cell and recording the temperature with both a thermocouple and the IR sensor. The calibrated IR-based temperature measurements aligned closely with thermocouple measurement with an error less than 1 K. To further evaluate the thermal gradient between the rear encapsulation and the actual PV cell, a control measurement was performed using a second encapsulation equipped with a solar thermal absorber (*Alanod EtaPlus*) and a thermocouple. The resulting temperature

differences, presented in Figure S7, confirm that the true maximum cell temperature of the GaAs PV was not reached during the experiments. Temperature readings for both the thermocouples and the IR sensor were recorded at a frequency of 1 Hz. Each experiment continued until thermal equilibrium was reached, defined as a temperature gradient below 1 K per h. Thermal and electrical characterisations were performed concurrently under illumination from the same solar simulator. Thermal efficiency was calculated from the rate of temperature increase in the water chamber, taking into account the thermal mass of the water. To reduce noise while preserving the trend, the temperature gradient was averaged over 25-s intervals. The thermal mass was determined by weighing the water in the absorber chamber (16.6 g) and multiplying by the specific heat capacity of water (4190 J/kg/K). Variations in heat capacity with temperature were neglected, and pressure was considered constant due to the use of an expansion tube. Uniform temperature distribution within the water chamber was assumed, facilitated by natural convection. Thermal efficiency was calculated relative to the total direct energy input of 10 W provided by the calibrated solar simulator. Initial transients during the heating phase were excluded from the efficiency analysis to ensure that only steady-state behaviour was considered.

The solar simulator is calibrated to the AM1.5G spectrum, which is standard for commercial simulators, and all electrical and thermal efficiencies are calculated based on the total calibrated irradiance. AM1.5D is therefore used only for theoretical optical analysis relevant to concentrated systems, while AM1.5G is adopted for the experimental measurements to ensure consistency with the simulator output.

Author Contributions

B.L. and G.H. developed the concept and research methodology. B.L. (lead) and G.H. designed the prototype. B.L. fabricated the prototype and conducted the experiment. B.L. and G.H. and B.S.R. conducted analysis on the research results. All authors contributed to writing and revising the manuscript. G.H. directed and supervised this project. The authors also wanted to thank Dr. Dmitry Busko for the support on calibrating the spectrum distribution of the solar simulator.

Acknowledgements

The authors gratefully acknowledge financial support received from: i) Helmholtz Investigator Group. ii) the Helmholtz Association Research Field Energy: Program Materials and Technologies for the Energy Transition (Topic 1 Photovoltaics and Wind Energy, ref. 38.01.04); iii) the Karlsruhe School of Optics and Photonics (KSOP); iv) KIT YIG-Prep-Pro project.

Open access funding enabled and organized by Projekt DEAL.

Conflicts of Interest

The authors declare no conflicts of interest.

Data Availability Statement

The data that support the findings of this study are available from the corresponding author upon reasonable request.

References

1. Innovation Landscape for Smart Electrification: Power-to-Heat and Cooling-Status. International Renewable Energy Agency, IRENA, accessed April 1, 2025, https://www.irena.org/Innovation-landscape-for-smart-electrification/Power-to-heat-and-cooling/Status.

2. Renewables 2024: Analysis and forecast to 2030, International Energy Agency, accessed April 1, 2025, https://www.iea.org/reports/renewables-2024.

3. Emissions Trends and Drivers, In: Climate Change 2022 - Mitigation of Climate Change: Working Group III Contribution to the Sixth Assessment Report of the Intergovernmental Panel on Climate Change (Intergovernmental Panel on Climate Change, 2023); pp. 215–294.

4. SunPower Maxeon 7, SUNPOWER, accessed August 14, (2025), https://cdn.prod.website-files.com/6627b4a16340c535bfabf896/668bef1148a5bfbf75c79fbe_Sunpower.pdf.

5. Abora, accessed August 12, 2025, https://abora-solar.com/.

6. A. Mellor, D. Alvarez, I. Guarracino, et al., "Roadmap for the Next-Generation of Hybrid Photovoltaic-Thermal Solar Energy Collectors," *Solar Energy* 174 (2018): 386–398.

7. G. Huang, S. R. Curt, K. Wang, and C. N. Markides, "Challenges and Opportunities for Nanomaterials in Spectral Splitting for High-Performance Hybrid Solar Photovoltaic-Thermal Applications: A Review," *Nano Materials Science* 2, no. 3 (2020): 183–203.

8. Technology Position Paper: PVT Collectors and System Concepts. IEA Solar Heating and Cooling Technology Collaboration Programme, Solar Heating & Cooling Programme, accessed April 1, 2025, https://www.iea-shc.org/Data/Sites/1/publications/IEA-SHC-Task60-PVT-Technology-Position-Paper.pdf.

9. M. A. Green and K. Emery, "Solar Cell Efficiency Tables," *Progress in Photovoltaics: Research and Applications* 32, no. 7 (2024): 425–441.

10. C. Sun, Y. Zou, C. Qin, B. Zhang, and X. Wu, "Temperature Effect of Photovoltaic Cells: A Review," *Advanced Composites and Hybrid Materials* 5, no. 4 (2022): 2675–2699.

11. X. Ju, C. Xu, X. Han, X. Du, G. Wei, and Y. Yang, "A Review of the Concentrated Photovoltaic/Thermal (CPVT) Hybrid Solar Systems Based on the Spectral Beam Splitting Technology," *Applied Energy* 187 (2017): 534–563.

12. A. Mojiri, R. Taylor, E. Thomsen, and G. Rosengarten, "Spectral Beam Splitting for Efficient Conversion of Solar Energy—A Review," *Renewable and Sustainable Energy Reviews* 28 (2013): 654–663.

13. M. Herrando, K. Wang, G. Huang, et al., "A Review of Solar Hybrid Photovoltaic-Thermal (PV-T) Collectors and Systems," *Progress in Energy and Combustion Science* 97 (2023): 101072.

14. H. Liang, F. Wang, L. Yang, Z. Cheng, Y. Shuai, and H. Tan, "Progress in Full Spectrum Solar Energy Utilisation by Spectral Beam Splitting Hybrid PV/T System," *Renewable and Sustainable Energy Reviews* 141 (2021): 110785.

15. L. Huaxu, W. Fuqiang, C. Ziming, S. Yong, L. Bo, and P. Yuzhai, "Performance Study on Optical Splitting Film-Based Spectral Splitting Concentrated Photovoltaic/Thermal Applications Under Concentrated Solar Irradiation," *Solar Energy* 206 (2020): 84–91.

16. T. P. Otanicar, S. Theisen, T. Norman, H. Tyagi, and R. A. Taylor, "Envisioning Advanced Solar Electricity Generation: Parametric Studies of CPV/T Systems with Spectral Filtering and High Temperature PV," *Applied Energy* 140 (2015): 224–233.

17. R. Wingert, H. O'Hern, M. Orosz, P. Harikumar, K. Roberts, and T. Otanicar, "Spectral Beam Splitting Retrofit for Hybrid PV/T Using Existing Parabolic Trough Power Plants for Enhanced Power Output," *Solar Energy* 202 (2020): 1–9.

18. R. A. Taylor, T. Otanicar, and G. Rosengarten, "Nanofluid-Based Optical Filter Optimisation for PV/T Systems," *Light: Science & Applications* 1, no. 10 (2012): e34–e34.

19. C. Pandey, M. Wu, A. Oyeniran, et al., "Numerical Study of a Parabolic-Trough CPV-T Collector with Spectral-Splitting Liquid Filters," *Frontiers in Energy* 19 (2025): 949–968.

20. L. Huaxu, W. Fuqiang, Z. Dong, et al., "Experimental Investigation of Cost-Effective ZnO Nanofluid Based Spectral Splitting CPV/T System," *Energy* 194 (2020): 116913.

21. L. Huaxu, W. Fuqiang, L. Dong, Z. Jie, and T. Jianyu, "Optical Properties and Transmittances of ZnO-Containing Nanofluids in Spectral Splitting Photovoltaic/Thermal Systems," *International Journal of Heat and Mass Transfer* 128 (2019): 668–678.

22. S. S. Chougule, A. Srivastava, G. G. Bolegave, B. A. Gaikwad, P. M. Shirage, and C. N. Markides, "Next-Generation Solar Technologies: Unlocking the Potential of Ag-ZnO Hybrid Nanofluids for Enhanced Spectral-Splitting Photovoltaic-Thermal Systems," *Renewable Energy* 236 (2024): 121405.

23. W. An, J. Zhang, T. Zhu, and N. Gao, "Investigation on a Spectral Splitting Photovoltaic/Thermal Hybrid System Based on Polypyrrole Nanofluid: Preliminary Test," *Renewable energy* 86 (2016): 633–642.

24. X. Xia, X. Cao, N. Li, B. Yu, and H. Liu, "Study on a Spectral Splitting Photovoltaic/Thermal System Based on CNT/Ag Mixed Nanofluids," *Energy* 271 (2023): 127093.

25. S. S. Chougule, B. A. Gaikwad, A. Inbaoli, A. Ajayan, S. K. Saha, and P. Estellé, "Hybrid Au-ZnO/(Water-Ethylene Glycol)-Nanofluid Based PV/T Spectral Beam Splitter for Efficient Photo-Harvesting," *Energy* 331 (2025): 137055.

26. M. U. Sajid and Y. Bicer, "Nanofluids as Solar Spectrum Splitters: A Critical Review," *Solar Energy* 207 (2020): 974–1001.

27. G. Huang, K. Wang, S. R. Curt, B. Franchetti, I. Pesmazoglou, and C. N. Markides, "On the Performance of Concentrating Fluid-Based Spectral-Splitting Hybrid PV-Thermal (PV-T) Solar Collectors," *Renewable Energy* 174 (2021): 590–605.

28. G. Huang, K. Wang, and C. N. Markides, "Efficiency Limits of Concentrating Spectral-Splitting Hybrid Photovoltaic-Thermal (PV-T) Solar Collectors and Systems," *Light: Science & Applications* 10, no. 1 (2021): 28.

29. Government of Canada, Heating and Cooling with a Heat Pump, accessed August 12, 2025, https://natural-resources.canada.ca/energy-efficiency/energy-star/heating-cooling-heat-pump.

30. Statistics Denmark, Energy Prices in 2024, accessed August 12, 2025, https://www.dst.dk/en/Statistik/emner/miljoe-og-energi/energiforbrug-og-energipriser/energipriser.

31. G. Huang and C. N. Markides, "Spectral-Splitting Hybrid PV-Thermal (PV-T) Solar Collectors Employing Semi-Transparent Solar Cells as Optical Filters," *Energy Conversion and Management* 248 (2021): 114776.

32. P. Singh and N. M. Ravindra, "Temperature Dependence of Solar Cell Performance—An Analysis," *Solar Energy Materials & Solar Cells* 101 (2012): 36–45.

33. M. I. Hossain, A. Bousselham, F. H. Alharbi, and N. Tabet, "Computational Analysis of Temperature Effects on Solar Cell Efficiency," *Journal of Computational Electronics* 16 (2017): 776–786.

34. M. Abdelhamid, B. K. Widyolar, L. Jiang, et al., "Novel Double-Stage High-Concentrated Solar Hybrid Photovoltaic/Thermal (PV/T) Collector with Nonimaging Optics and GaAs Solar Cells Reflector," *Applied Energy* 182 (2016): 68–79.

35. NREL, Champion Photovoltaic Module Efficiency Chart, 2026, https://www.nlr.gov/pv/module-efficiency.

36. SunPower C60, accessed August 12, 2025, http://eshop.terms.eu/_data/s_3386/files/1379942540-sunpower_c60_bin_ghi.pdf.

Supporting Information

Additional supporting information can be found online in the Supporting Information section.

Supporting File: adom71055-sup-0001-SuppMat.pdf.